Ultrasonic guided waves in cortical bone modeled as a functionally graded anisotropic tube

Cécile Baron

ACOUSTICS 2012

Ultrasonic guided waves in cortical bone modeled as a functionally graded anisotropic tube

C. Baron

CNRS - Aix Marseille Univ, 163 avenue de Luminy, 13288 Marseille, France
cecile.baron@univmed.fr

The human cortical bone is a heterogeneous medium: it is multiscale and multicomponent. It can be seen as a biphasic material, pores full of marrow in a bone matrix, with an increasing porosity from periosteum to endosteum. This porosity gradient reveals itself representative of loss of mass, changes in geometry (thinning) and variations in structure (porosity) which occur with aging and are determinants of bone strength. By applying a homogenization process, cortical bone can be considered as an anisotropic functionally graded material with variations in material properties. A semi-analytical method based on the sextic Stroh formalism is proposed to solve the wave equation in an anisotropic functionally graded tubular waveguide, without using a multilayered model to represent the structure. This method provides an analytical solution called the matricant and explicitly expressed under the Peano series expansion form.
Our findings indicate that ultrasonic guided waves are sensitive to the age-related evolution of realistic gradients in human bone properties across the cortical thickness and have their place in a multimodal clinical protocol.

1 Introduction

It is now widely accepted that bone strength relies on two main factors: bone density and bone quality. Thus, accurate information is needed on the quantity of bone, the way it is organized and the mechanical quality of its constituent materials (elastic properties) in order to accurately evaluate fracture risk, to optimize treatment (time and dosage) and to reduce adverse effects.

It would appear that bone quantity alone is not sufficient to evaluate bone fragility, and that bone geometry and quality are key factors which significantly affect bone strength. At the same time, as imaging techniques become more and more accurate, a newly visible characteristic of bone is emerging: intracortical porosity changes gradually across the thickness of long bones [7, 21, 11, 10]. When homogenization methods are applied to cortical bone, it can be viewed as a functionally graded material at mesoscopic scale. Among the changes in cortical bone due to aging, there is a joint process accentuated by osteoporosis: trabecularization of the endosteal part leading to thinning of the cortex. Therefore the gradient (spatial variation) of intracortical porosity is a parameter representative of increased variation in porosity across a reduced thickness, and should be relevant to evaluate the combined effect of thinning and trabecularization. This gradient of intracortical porosity induces gradients of material properties (mass density and stiffness coefficients). Thus, characterizing the gradient of the bone properties across the cortical thickness, will provide information on structure (porosity), geometry (thickness) and material (stiffness). A semi-analytical method is proposed to solve the wave equation in an FGM waveguide. This method, based on the Stroh formalism, allows us to avoid a multilayered media approximation and to consider a cylindrical geometry in association with an anisotropic material. Here cortical bone is represented by a transversely isotropic tube in vacuum. The dispersion curves of the guided waves are explored to evaluate the sensitivity of these waves to a realistic variation in intracortical porosity.

2 Materials and Methods

The model takes into account the anisotropy and the heterogeneity of cortical bone: it is considered as transversely isotropic with linearly varying material properties.

2.1 Material properties gradient

Here, every attempt was made to model realistic variation in porosity across the cortical thickness. Based on previous work reported on femoral cortical bone samples from skeletons [6, 7], we focus on a solely female population (86 subjects) restricted to three age ranges [30-39], [60-69] and [80-99] year old. We use these authors' 3-point measurement of porosity (periosteal, mid-cortical and endosteal regions) to infer the evolution of porosity across the cortical thickness.

Then, the evolution of intracortical porosity (microscopic scale) is translated into a variation in the elastic properties of the bone at the mesoscopic level by using the regression models (size of the mesodomain $L = 0.5$ mm) proposed by Grimal and colleagues [10]. Thereby, the Young's and shear moduli and the Poisson ratios are expressed as a function of porosity.

Porosity varies with position across the thickness of the bone, and consequently the Young's and shear moduli and Poisson ratios are also dependent on the spatial variable across the thickness (r-variable for the tube), except for ν_{TL}, which is assumed to be constant at 0.3. Then we deduce the five independent stiffness coefficients as five spatially-dependent functions.

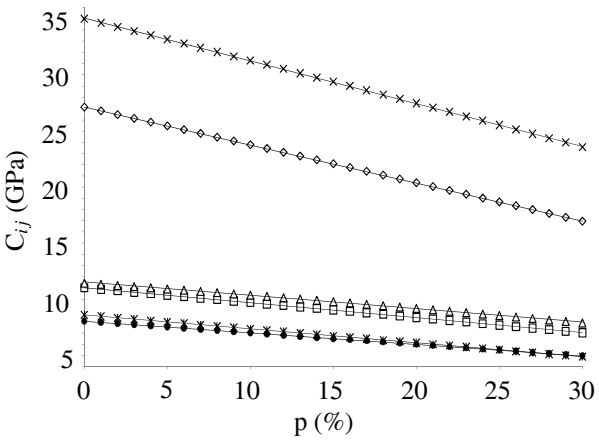

Figure 1: Variation of the stiffness coefficients over the porosity: $c_{11} = c_{22}$ ($\diamond$), c_{12} ($\square$), $c_{13} = c_{23}$ (Δ), c_{33} ($\times$), $c_{44} = c_{55}$ ($*$), c_{66} ($\bullet$).

Figure 1 shows that the stiffness coefficients can be supposed to linearly vary according to porosity across the cortical thickness for each age group. A linear regression provides an affine function representing the evolution of the stiffness coefficients across the cortical thickness.

A classical mixture law is used to obtain mass density as a function of spatial variable r. We assume that the pores are filled with water considered as a perfect fluid:

$$\rho(r) = \rho_{bone}(1 - p(r)) + \rho_{water}p(r); \quad (1)$$

with p the porosity, $\rho_{bone} = 1.9$ g/cm^3 and $\rho_{water} = 1$

g/cm^3.

The maximum and minimum values of the elastic properties (stiffness coefficients and mass density) are reported in Table 1.

		[30-39]	[60-69]	[80-99]
c_{11}	per.	26.10	25.69	25.15
(GPa)	end.	24.40	22.03	18.06
c_{12}	per.	10.64	10.48	10.26
(GPa)	end.	9.97	9.03	7.47
c_{13}	per.	11.16	11.02	10.83
(GPa)	end.	10.57	9.75	8.37
c_{33}	per.	33.90	33.44	32.83
(GPa)	end.	31.99	29.32	24.86
c_{44}	per.	8.22	8.07	7.87
(GPa)	end.	7.60	6.73	5.28
c_{66}	per.	7.73	7.61	7.44
(GPa)	end.	7.22	6.49	5.29
ρ	per.	1.87	1.86	1.85
(g/cm^3)	end.	1.83	1.76	1.66

Table 1: Elastic properties of cortical bone at the periosteal boundary (per.) and at the endosteal boundary (end.).

2.2 Waveguide geometry

Thickness of the tube was taken from [7]. Previous findings [8, 9] have established that the outer diameter remains the same after 30 years; in this study, it is fixed at 24 mm and the thinning of the cortical wall with age is represented by an increase in the inner diameter to reach the thickness measured by Bousson and colleagues [7]. The geometry of the tube for the three age ranges studied is reported in Table 2.

	t (mm)	a_0 (mm)	a_q (mm)	t/a_q
[30-39]	4.368	7.64	12	0.36
[60-69]	3.104	8.9	12	0.26
[80-99]	2.502	9.5	12	0.21

Table 2: Geometry of the tube waveguide for three ranges of age.

2.3 Wave propagation in radially FGM tube

We consider an elastic waveguide of thickness t placed in vacuum. The coordinate systems (r, θ, z) for the tube are defined with the z-axis corresponding to the axis of the long bone and r representing the spatial variable along the cortical thickness.

The radius of the tube r varies from a_0 to a_q, respectively the inner and outer radius of the tube.

The elastic waveguide is considered to be anisotropic and is liable to present continuously varying properties across its thickness ($\mathbf{e}_r$-axis). These mechanical properties are represented by the stiffness tensor $\mathbb{C} = \mathbb{C}(r)$ and the mass density $\rho = \rho(r)$.

System equations

The momentum conservation equation associated with the constitutive law of linear elasticity (Hooke's law) gives the following equations:

$$\begin{cases} \mathrm{div}\sigma = \rho \dfrac{\partial^2 \mathbf{u}}{\partial t^2}, \\ \sigma = \dfrac{1}{2}\mathbb{C}\,(\mathrm{grad}\mathbf{u} + \mathrm{grad}^T\mathbf{u}), \end{cases} \tag{2}$$

where $\mathbf{u}$ is the displacement vector and σ the stress tensor.

We seek to solve the wave equation for displacement vector ($\mathbf{u}$) and radial traction vector ($\sigma_r = \sigma.\mathbf{e}_r$) expressed in the cylindrical coordinates (r, θ, z) with the basis $\{\mathbf{e}_r, \mathbf{e}_\theta, \mathbf{e}_z\}$:

$$\begin{aligned} \mathbf{u}(r, \theta, z; t) &= \mathbf{U}^{(n)}(r) \exp \imath\,(n\theta + k_z z - \omega t)\,, \\ \sigma_r(r, \theta, z; t) &= \mathbf{T}^{(n)}(r) \exp \imath\,(n\theta + k_z z - \omega t)\,; \end{aligned} \tag{3}$$

with k_z the axial wavenumber and n the circumferential wavenumber.

We distinguish two types of waves propagating in a cylindrical waveguide: *circumferential waves* and *axial waves*. *Circumferential waves* are waves traveling in planes perpendicular to the axis direction. They correspond to $u_z(r) = 0\,(\forall r)$, $k_z = 0$ and $n = k_\theta a_q$. *Axial waves* are waves traveling along the axis direction, the circumferential wavenumber is an integer $n = 0, 1, 2, ...$ Among the *axial waves*, we distinguish three types of modes numbered with two parameters (n, m) representing the circumferential wavenumber and the order of the branches: longitudinal (L), flexural (F) and torsional (T) modes. The longitudinal and torsional modes are axially symmetric ($n = 0$) and denoted $L(0, m)$ and $T(0, m)$. The flexural modes are non-axially symmetric ($n \geq 1$) and are denoted $F(n, m)$. In this paper, we focus on longitudinal and first flexural modes ($n = 1$).

A closed-form solution: the matricant

Introducing the expression (3) into the equation (2), we obtain the wave equation in the form of a second-order differential equation with non-constant coefficients. In the general case, there is no analytical solution to the problem thus formulated. Most current methods of solving the wave equation in unidirectionally heterogeneous media are derived from the Thomson-Haskell method [22, 12]. These methods are appropriate for multilayered structures. However, for continuously varying media, these techniques replace the continuous profiles of properties by step-wise functions, thereby making the problem approximate, even before the resolution step. The accuracy of the solution, like its validity domain, are thus hard to evaluate. Moreover, a multilayered model of functionally graded waveguides creates "virtual" interfaces likely to induce artefacts. Lastly, for generally anisotropic cylinders, the solutions cannot be expressed analytically, even for homogeneous layers [14, 19].

To solve the exact problem, that is, to maintain the continuity of the variation in properties , and to take into account the anisotropy of cylindrical waveguides, we write the wave equation under the sextic Stroh formalism [20] in the form of an ordinary differential equations system with non-constant coefficients for which an analytical solution exists: the matricant [16, 1].

Hamiltonian form of the wave equation In the Fourier domain, the wave equation can be written as:

$$\frac{d}{dr}\eta(r) = \frac{1}{r}\mathbf{Q}(r)\eta(r). \tag{4}$$

The components of the state-vector $\eta(r)$ are the components of the displacement vector $\mathbf{u}$ and the components of the traction vector σ_r. As for the matrix $\mathbf{Q}(r)$, it contains all the information about heterogeneity: it is expressed from the stiffness coefficients of the waveguide in the cylindrical system of coordinates and from two acoustical parameters (wavenumber k_z, angular frequency ω).

Explicit solution: the Peano expansion of the matricant The wave equation thus formulated has an analytical solution expressed between a reference point r_0 and some point along the cortical thickness direction r. This solution is called the matricant and is explicitly written in the form of the Peano series expansion:

$$\mathbf{M}(r, r_0) = \mathbf{I} + \int_{r_0}^{r} \mathbf{Q}(\varsigma)d\varsigma + \int_{r_0}^{r} \mathbf{Q}(\varsigma) \int_{r_0}^{\varsigma} \mathbf{Q}(\varsigma_1)d\varsigma_1 d\varsigma + ..., \tag{5}$$

where $\mathbf{I}$ is the identity matrix of dimension $(6, 6)$. If the matrix $\mathbf{Q}(r)$ is bounded in the study interval, these series are always convergent [1]. The components of the matrix $\mathbf{Q}$ are continuous in r and the study interval is bounded (thickness of the waveguide), consequently the hypothesis is always borne out. The matricant verifies the propagator property [1]:

$$\eta(r) = \mathbf{M}(r, r_0)\eta(r_0). \tag{6}$$

Free boundary conditions The waveguide is considered to be in vacuum, so the traction vector σ_r defined in (3) is null at both interfaces. Using the propagator property of the matricant through the thickness of the structure, equation (6) is written as $\eta(r_0 + t) = \mathbf{M}(r_0 + t, r_0)\eta(r_0)$ with $r_0 = a_0$. Factorizing the matricant $\mathbf{M}(r_0 + t, r_0)$ under four block matrices of dimension $(3, 3)$, equation 6 becomes:

$$\begin{pmatrix} \mathbf{u}(r = r_0 + t) \\ \mathbf{0} \end{pmatrix} = \begin{pmatrix} \mathbf{M}_1 & \mathbf{M}_2 \\ \mathbf{M}_3 & \mathbf{M}_4 \end{pmatrix} \begin{pmatrix} \mathbf{u}(r = r_0) \\ \mathbf{0} \end{pmatrix}. \tag{7}$$

Equation (7) has non-trivial solutions for $\det\mathbf{M}_3 = 0$. The components of $\mathbf{M}_3$ are bivariate polynomials in (s_z, ω) or (k_z, ω). Consequently, seeking the zeros of $\det\mathbf{M}_3$ amounts to seeking the pairs of values (k_z, ω) which describe the dispersion curves of guided waves propagating in a tube.

3 Results

3.1 Gradient of porosity

The variation in porosity across the cortical thickness and its age-related evolution are presented in Table 3.

	p% per. (%)	p% mid. (%)	p% end. (%)	*grad* (%/mm)
[30-39]	3.1	4.4	8.1	1.145
[60-69]	4.3	11.5	15.1	3.479
[80-99]	5.9	17.5	26.8	8.353

Table 3: Age-related regional evolution of intracortical porosity and gradient.

Figure 2 shows that a linear profile is a good approximation to model porosity changes. For every age range, $p\% = a\xi + b$, where ξ is the spatial variable along the cortical thickness, $(a, b) \in \Re^2$.
The porosity gradient (%/mm) is deduced from an estimation of the slope a for each age class (Table 3).

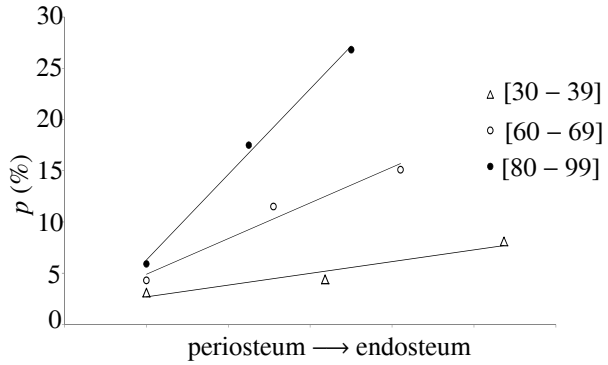

Figure 2: Variation of the porosity along the cortical thickness: linear regression for each range of age ($R^2 \geq 0.9$).

Figure 2 clearly shows that porosity sharply increases with age in the endosteal region, whereas it remains fairly stable in the periosteal region. Moreover, cortical thickness greatly decreases with age, from adulthood to old age. These two processes identified by Bousson [6, 7], are linked under the name trabecularization of the endosteal region.

3.2 Sensitivity of guided waves to the gradient of material properties

The effect of a realistic intracortical porosity gradient on guided wave propagation was investigated to determine how sensitive the guided waves are to the age-related evolution of long bone strength; in particular, whether they are sensitive both to thinning of the cortex and to increased endosteal porosity during aging. We compared the ultrasonic guided waves' interaction with three tubular waveguides modeling the diaphysis of the femur at three different age ranges: [30-39], [60-69] and [80-99] [7]. Waveguides dimensions are reported in Table 2. The dispersion curves are plotted as functions of the frequency-thickness product in the usual range for the study of ultrasonic waves in long bones [5, 21, 17]. For guided waves in long bones, the typical frequency range is between 50 kHz to 350 MHz [15] to generate wavelengths greater than the cortical thickness [5]. Consequently, the frequency-thickness product to be considered is roughly [0.2, 1.5] MHz.mm for [30-39], [0.15, 1.1] MHz.mm for [60-69] and [0.125, 0.875] MHz.mm for [80-99].

The dispersion curves of longitudinal and flexural modes propagating in tubes show measurable differences throughout aging (Figure 3).

The cut-off frequencies of all the modes are distinct for the three age ranges considered (Table 4). The phase velocities are also significantly different: for instance, the discrepancy between the $F(1, 3)$-mode phase velocity for [80-99] and the $F(1, 3)$-mode phase velocity for [30-39] is about 420 m/s. All these differences correspond to several thousand meters per second, which are experimentally measurable quantities.

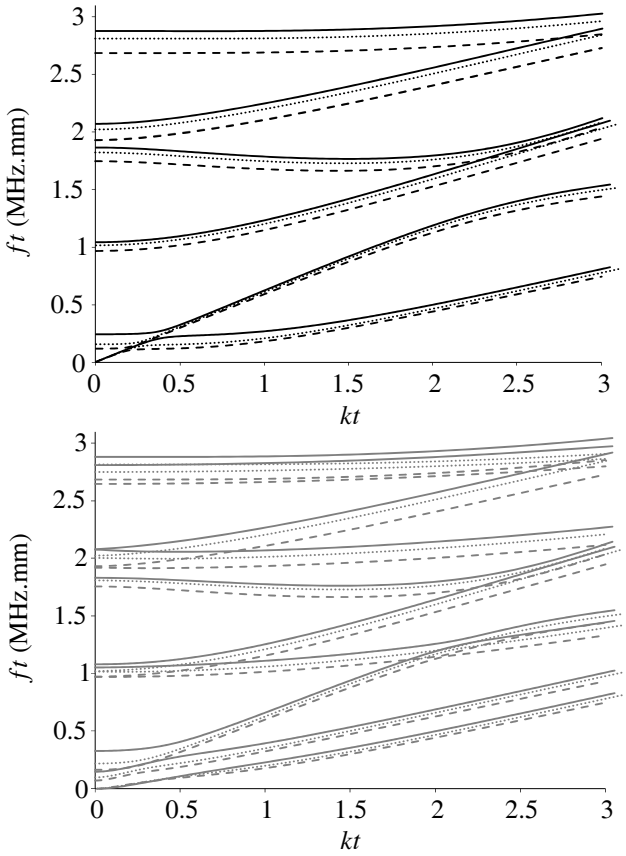

Figure 3: Dispersion curves of the eight first longitudinal modes (in black) and the ten first flexural (in grey) modes propagating in a transversely isotropic tube, for three ranges of age: [30-39] in straight line, [60-69] in dots and [80-99] in dotted line.

	$\Delta f_{30/60}$ (kHz)	$\Delta f_{60/80}$ (kHz)	$\Delta f_{30/80}$ (kHz)
L(0,2)	4.9	3.4	8.3
L(0,3)	88.3	60.3	148.6
F(1,2)	2.9	2.2	5.1
F(1,3)	4.5	4	8.4
F(1,4)	87.2	60.1	147.3
F(1,5)	80.8	59.7	140.5

Table 4: Variations of cut-off frequencies for longitudinal and flexural modes with aging.

4 Discussion

The Stroh formalism used in this study has several advantages. First, it allows ultrasound propagation to be investigated in a continuously varying medium (FGM) instead of approximating it by a multilayered medium, thus avoiding potential round-off errors and artefacts which cannot be estimated. It provides an exact solution to the exact problem, and the degree of round-off error is manageable [1]. Furthermore, this formalism is numerically stable and is applicable to planar and tubular geometries whatever the degree of anisotropy of the material. The conventional methods used to solve the wave equation are unable to deal with cylindrical coordinates coupled with general anisotropy. The Stroh formalism is one of the only ways to provide an analytical solution (Peano expansion of the matricant) to the wave equation in a cylindrical structure whatever the anisotropy of the material [18]. Moreover, fluid-loading of the waveguide here can be treated as in the case of the plate [3]. The advantages of this formalism in the context of bone characterization are clear, since long bone can be realistically modeled as an FGM orthotropic tube surrounded by blood and full of marrow. In addition, because this method takes into account actual variations in material properties of long bones, it could prove useful as a reference to validate models which do not allow for the gradient of material properties, confirming the range of validity (frequency domain, thickness range, order of the modes) of the results yielded by such simplified models.

Bone fragility has long been known to be related to the quantity of material (bone density), its quality (stiffness) and its organization (geometry and micro-architecture). An accurate evaluation of fracture risk has to assess these three parameters together. As cortical bone ages, endosteal trabecularization induces thinning of the cortex. Thus, the spatial variation in porosity across the cortical thickness revealed during aging can be taken as the "missing" parameter to represent bone quality. As previously pointed out, the gradient of material properties (density and stiffness coefficients) reflects the spatial distribution of the quantity and quality of bone across the cortical thickness. Looking at the dispersion curves obtained here for the tube, this discrepancy between the different age ranges appears to be experimentally measurable. Thus, this study indicates that the gradient of homogenized material properties can be evaluated from measured ultrasound velocities.

Our work demonstrates the sensitivity of guided waves to realistic variations in the intrinsic properties of human cortical bone: porosity, density, stiffness, as revealed by the gradient in material properties. Nevertheless, it remains difficult to establish a reliable criterion to apply in a clinical protocol. Careful consideration needs to be given to choosing appropriate anatomical sites for ultrasonic evaluation.
Our model could usefully be extended. Several realistic characteristics can easily be added to the formalism we use. Firstly, how soft tissue affects wave propagation can be modeled by fluid-loading, as examined in a recent paper [3]. Secondly, the gradual variation in the intrinsic properties of the bone matrix described in [13] can be included in the homogenization step and would contribute to the mesoscopic gradient of bone properties.

5 Conclusion

The gradient of material properties appears here to be relevant to evaluating age-related changes in cortical bone, particularly in the context of osteoporosis and therapeutic follow-up. This paper describes an original method applied to bone characterization able to take into account the heterogeneity (porosity gradient) and the anisotropy (orthotropy) of the material as well as the tubular geometry of the structure, even under *in-vivo* conditions (soft tissue).

Ultrasound evaluation appears a good candidate to characterize long bone (structure, geometry and material); however, the potential of *in-vivo* techniques that take into account the influence of soft tissue and marrow needs to be further explored.

The results we obtain are promising, but the method should be extended, in particular with a view to solving the inverse

problem. An *in-vitro* experimental program would validate the feasibility of the ultrasound measurements on bone samples of different ages. It could also evaluate the relevance of using an *in-vivo* characterization of the gradient of properties across the cortical thickness to determine bone strength and the risk of fracture.

References

[1] C. Baron *Le developpement en serie de Peano du matricant pour l etude de la propagation d ondes en milieux continument variables - Peano expansion of the matricant to study elastic wave propagation in continuously heterogeneous media*. Ph.D. thesis, Universite Bordeaux 1, France, (2005)

[2] C. Baron "Propagation of elastic waves in an anisotropic functionally graded hollow cylinder in vacuum", *Ultrasonics*, **51**, 123-130 (2011)

[3] C. Baron, S. Naili "Propagation of elastic waves in a fluid-loaded anisotropic functionally graded waveguide: Application to ultrasound characterization". *Journal of Acoustical Society of America*, **127**, 1307-1317 (2010)

[4] C. Baron, M. Talmant, P. Laugier "Effect of porosity on effective diagonal stiffness coefficients (c_{ii}) and anisotropy of cortical at 1 MHz: A finite-difference time domain study" *Journal of Acoustical Society of America*, **122**, 1810–1817 (2007)

[5] E. Bossy, M. Talmant, P. Laugier "Three-dimensional simulations of ultrasonic axial transmission velocity measurement on cortical models" *Journal of Acoustical Society of America*, **115**, 2314-2324 (2004)

[6] V. Bousson, C. Bergot, A. Meunier, C. Parlier-Cuau, A.M. Laval-Jeantet, J.D. Laredo "CT of the Middiaphyseal Femur: Cortical Bone Mineral Density end Relation to Porosity" *Radiology*, **217**, 179-187 (2000)

[7] V. Bousson, A. Meunier, C. Bergot, E. Vicaut, M.A. Rocha, M.H. Morais, A.M. Laval-Jeantet, J.D. Laredo "Distribution of intracortical porosity in human midfemoral cortex by age and gender" *Journal of Bone and Mineral Reasearch*, **16**, 1308-1317 (2001)

[8] D.R. Carter, M.C.H. Van Der Meulen, G.S.Beaupre "Mechanical Factors in Bone Growth and Development" *Bone*, **18**, 5S-10S (1996)

[9] S.A. Feik , D.L. Thomas, J.G. Clement "Age trends in remodeling of the femoral midshaft differ between the sexes" *Journal of Orthopaedic Research*, **14**, 590-597 (2005)

[10] G. Grimal, K. Raum, A. Gerisch, P. Laugier. "A determination of the minimum sizes of representative volume elements for the prediction of cortical bone elastic properties" *Biomechanics and Modeling in Mechanobiology* **OnLineFirst**^{TM}, 1-13 (2011)

[11] G. Haiat, S. Naili, G. Grimal, M. Talmant "Influence of a gradient of material properties on ultrasonic wave propagation in cortical bone: Application to axial transmission" *Journal of Acoustical Society of America* **125**, 4043-4052 (2009)

[12] N.A. Haskell "The dispersion of surface waves on multilayered media" *Bulletin of the Seismological Society of America* **43**, 377-393 (1953)

[13] S. Lakshmanan, A. Bodi, K. Raum "Assessment of anisotropic tissue elasticity of cortical bone from high-resolution, angular acoustic measurements" *IEEE Trans Ultrason Ferroelectr Freq Control* **54**, 1560-1570 (2007)

[14] I. Mirsky "Axisymmetric vibrations of orthotropic cylinders" *Journal of the Acoustical Society of America* **36**, 2106-2112 (1964)

[15] P. Moilanen, M. Talmant, V. Kilappa, P.H.P. Nicholson, S. Cheng, J. Timonen, P. Laugier "Modeling the impact of soft tissue on axial transmission measurements of ultrasonic guided waves in human radius" *Journal of the Acoustical Society of America* **124**, 2364-2373 (2008)

[16] M.C. Pease *Methods of Matrix Algebra*. Academic Press, New York (1965)

[17] V. Protopappas, D. Fotiadis, K. Malizos "Guided ultrasound wave propagation in intact and healing long bone" *Ultrasound in Medicine and Biology* **32**, 693-708 (2006)

[18] A. Shuvalov "A sextic formalism for three-dimensional elastodynamics of cylindrically anisotropic radially inhomogeneous materials" *Proceedings of the Royal Society of London A.* **459**, 1611-1639 (2003)

[19] K. Soldatos, Y. Jianqiao "Wave propagation in anisotropic laminated hollow cylinders of infinite extent" *Journal of the Acoustical Society of America* **96**, 3744-3752 (1994)

[20] A.N. Stroh "Steady state problems in anisotropic elasticity" *Journal of Mathematics and Physics* **41**, 77-103 (1962)

[21] A. Tatarinov, N. Sarvazyan, A. Sarvazyan "Use of multiple acoustic wave modes for assessment of long bones: model study" *Ultrasonics* **438**, 672-680 (2005)

[22] W.T. Thomson "Transmission of elastic waves through a stratified solid medium" *Journal of Applied Physics* **21**,89-93 (1950)